Ocean Retrievals for WindSat

Radiative Transfer Model, Algorithm, Validation

Thomas Meissner and Frank Wentz
Remote Sensing Systems
438 First Street, Suite 200, Santa Rosa, CA 95401, USA
meissner@remss.com, frank.wentz@remss.com

***Abstract*— We have developed an ocean retrieval algorithm for WindSat retrieving sea-surface wind speed and direction, sea-surface temperature (SST), columnar atmospheric water vapor, columnar liquid cloud water, and rain rate.**

The physical basis for the algorithm is the radiative transfer model (RTM). This model expresses the microwave brightness temperature (TB) in terms of SST, wind vector, and atmospheric profiles of temperature and moisture. The WindSat observations in conjunction with observations from other satellites or numerical weather prediction models are used to determine or refine the wind induced sea-surface emissivity component of the RTM.

For WindSat, the wind direction signal for vertical (v) and horizontal polarization (h) can be determined by taking the difference between forward and backward look, which allows a more accurate determination than using only the forward look, as atmospheric uncertainties cancel out.

A new feature of the WindSat ocean algorithm compared with algorithms for earlier instruments (SSM/I, TMI, AMSR-E) is the use of the 3rd and 4th Stokes brightness temperatures.

To retrieve wind direction, a maximum-likelihood approach finds a set of possible wind vector solutions (ambiguities) that minimize the difference between the observations and the radiative transfer model. A median filter selects the most likely ambiguity. We present retrievals for a 9-month period and compare to a variety of validation datasets (buoys, ship cruises, numerical weather prediction models, satellites). The performance of WindSat retrievals for SST T_S, wind speed W, water vapor V and cloud water L matches closely the ones from other microwave imagers. For wind speeds above 7 m/s, the WindSat wind direction error is below 20 deg. Accurate wind direction retrievals for wind speeds below 5 m/s are difficult due to the lack of sufficient signal size.

Keywords- WindSat; Radiative Transfer Model; Wind Direction Signal; Stokes Parameters; Ocean Wind Vector; Sea Surface Temperature, Water Vapor; Cloud Water; Validation.

I. Brightness Temperatures: Data Set, Calibration, Resampling

We have obtained 9 months of WindSat antenna temperatures from NRL (TDR version 146AFBBDA) comprising the time between July 2003 and April 2004. Using the values for spillover correction and antenna pattern correction (cross polarization correction) that were also provided by NRL (version March 2003) the antenna temperatures are transformed into ocean brightness temperatures (TBs).

We have calibrated the TBs to our AMSR radiative transfer model (RTM) [1] by comparing the measured TBs with RTM computed TBs. In order to do this, it is necessary to collocate the WindSat TBs with environmental data records (EDR). They are be obtained from other satellite measurements, the optimum interpolated Reynolds SST [2] or numerical weather prediction models.

We have identified and corrected across scan biases as well as biases resulting from errors in the hot load calibration.

It has been necessary to correct the polarization rotation angle between Earth and spacecraft polarization basis due to a misspecification of the spacecraft attitude i, [4]. We have also computed Faraday rotation and corrected the 3rd Stokes parameter at 10.7 GHz [3].

The TBs have been averaged and resampled to the resolution of the 10.7 GHz footprint. The observations are then averaged into 0.25^o latitude- longitude maps. A mask for land and sea ice is applied, the data are filtered for rain by discarding events for which TB (37H) is larger than 200 K, sun glitter and for radio frequency interference (RFI) [3].

II. Refinement of the Wind Induces Sea Surface Emissivity Model

A. Method

In our RTM, we use the specular sea surface emissivity based on the dielectric constant that was derived in [5]. The wind induced sea surface emissivity depends on SST, SSWS and SSWD. To refine the wind induced emissivity component of the RTM we have analyzed the difference between TBs that are measured from WindSat and the TBs that are computed form the RTM for a sea surface without wind. The emissivity can then be computed from the radiative transfer equation after correcting for the atmospheric component. The result is binned as function of SST, SSWS and SSWD. For deriving the wind induced sea surface emissivity accurately, it is essential to use very accurate values for the atmospheric parameters. Our collocation method uses wind, vapor and liquid cloud water from other microwave imagers (SSM/I, TMI, AMSR-E), that have been averaged into 0.25^o latitude- longitude maps, and that are closest in time but within 60 minutes of the WindSat observation.

B. *Wind Induced Isotropic Sea Surface Emissivity*

As a first step we consider the isotropic (direction independent) wind induced emissivity for vertical (v) and horizontal (h) polarization by averaging globally over a large number of wind directions. The emissivity signal arises due to large-scale roughness, small-scale roughness (Bragg scattering from capillary waves) and, at wind speeds above 7 m/s, the emissivity of sea foam. The result for 10.7 GHz is shown in Figure 1.

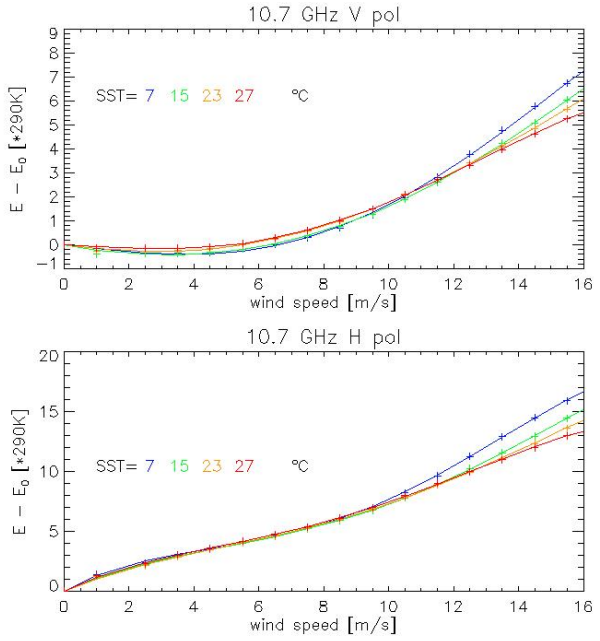

Figure 1. Wind induced isotropic sea surface emissivity at 10.7 GHz as function of SST and SSWS.

C. *Wind Direction Signal for V and H-pol from For-Aft Look*

As discussed in [6], the analysis of the 1st and 2nd harmonics of the wind direction signal for v and h-pol is very sensitive to errors in the atmospheric component entering the isotropic part (0th harmonic). The 2-look geometry of WindSat offers the opportunity to eliminate this large isotropic component. Unfortunately, in the WindSat mission, the earth incidence angles θ (EIA) between for and back scan can be different by up to 1°. It is therefore necessary to reference for and aft observation for a single Earth cell to the same EIA. This can be done by using the RTM to compute the TB difference between for and aft look that results from the EIA difference. The TBs for the for and aft looks, expanded up to 2nd harmonic, are:

$$T_{BFor} = A_0\left(\theta_{For};T_S,W,ATM\right)+\tau^2 T_{eff}A_1\cos\left(\varphi_{For}\right)+\tau^2 T_{eff}A_2\cos\left(2\varphi_{For}\right) \quad (1)$$
$$T_{BAft} = A_0\left(\theta_{Aft};T_S,W,ATM\right)+\tau^2 T_{eff}A_1\cos\left(\varphi_{Aft}\right)+\tau^2 T_{eff}A_2\cos\left(2\varphi_{Aft}\right)$$

$A_i, i=0,1,2$ are the harmonic coefficients, A_0 is the large isotropic component and $A_{1,2}$ the wind direction signal. ATM stands for the atmospheric profiles (pressure, temperature, humidity, cloud water density), τ is the atmospheric attenuation and T_{eff} an effective temperature of the ocean atmosphere system. The TB of the aft look corrected to the EIA of the for look is:

$$T_{BAft}{}' = T_{BAft} + F\left(\theta_{For};T_S,W,ATM\right) - F\left(\theta_{Aft};T_S,W,ATM\right) \quad (2)$$

F is the RTM model function. The isotropic parts A_0 of T_{BFor} and $T_{BAft}{}'$ are then identical and cancel out when taking the difference.

$$T_{BFor} - T_{BAft}{}' = \tau^2 T_{eff}A_1\left[\cos\left(\varphi_{For}\right)-\cos\left(\varphi_{Aft}\right)\right]+\tau^2 T_{eff}A_2\left[\cos\left(2\varphi_{For}\right)-\cos\left(2\varphi_{Aft}\right)\right] \quad (3)$$

We have assumed that T_S, W and the atmosphere are the same for and aft look and that the higher harmonics do not depend on the EIA.

This method basically eliminates all atmospheric errors resulting in a residuum of the fit for 1st and 2nd harmonics that is much smaller than for a 1-look radiometer [6]. The results for the 1st and 2nd harmonic together with a comparison with the 1-look microwave satellite analysis [6] and the JPL aircraft analysis [7] are shown in Figure 2.

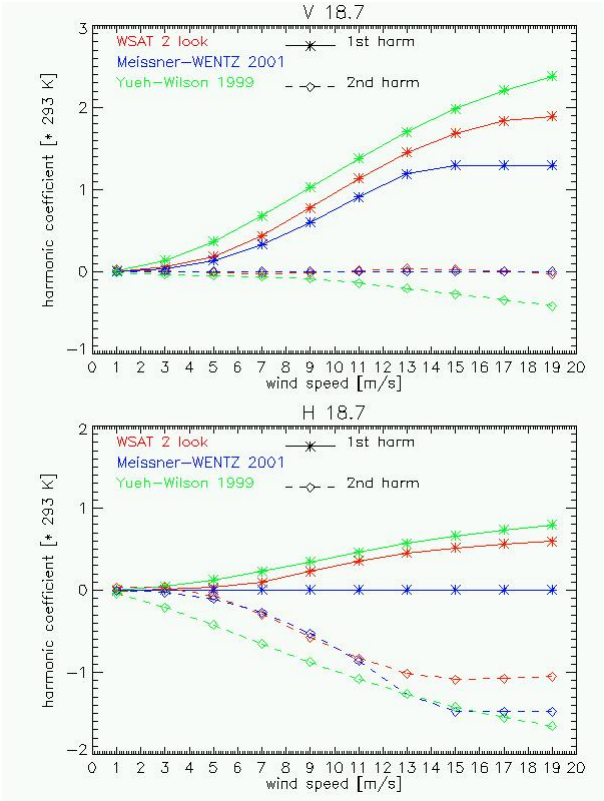

Figure 2. Wind direction signal for v and h-pol at 18.7 GHz from WindSat for – aft look anakysis and comparison with the results of [6]and [7].

D. *3rd and 4th Stokes Parameters*

The 3rd Stokes parameter is the differences between +45 and –45 polarized TB and the 4th Stokes parameter is the difference between left hand and right hand circular polarized TB. Therefore the isotropic atmospheric components cancel when taking the differences. The results of our analysis and a comparison with the JPL aircraft analysis [7] are shown in Figure 3. Our sign convention for the 4th Stokes parameter follows that of [10], which is opposite from what was used in [7].

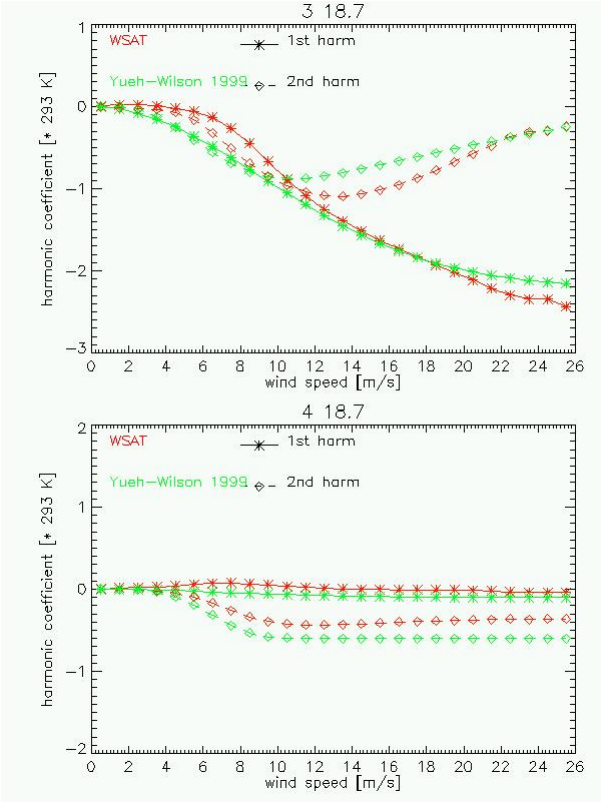

Figure 3. 3rd and 4th Stokes parameter at 18.7 GHz and comparison with [7].

At intermediate wind speeds (7 m/s), the magnitudes of both Stokes parameters from WindSat are significantly smaller (by more than 50%) than the ones from the aircraft flights [7]. WindSat does not show any 4th Stokes parameter at 37 GHz contrary to the prediction of the 2-scale models [8].

III. Ocean Retrieval Algorithm

A. *Multi-Sstage Regressions for SST ,SSWS, Columnar Water Vapor and Columnar Liquid Cloud Water*

Our algorithms for retrieving SST, scalar SSWS, columnar water vapor and columnar liquid cloud water were adapted form AMSR-E. Using our refined sea surface emissivity model (section II) and the atmospheric model from [1] we Monte Carlo simulate ocean brightness temperatures over a large training set of NCEP GDAS SST as well as atmospheric profiles for pressure, temperature, water vapor density and liquid cloud water. We let SSWS vary randomly and uniformly between 0 and 25 m/s, and SSWD randomly and uniformly between 0 and 360 deg. The data set contains more than 500,000 events that were taken over the whole ocean and contain one day of each month. When computing the TBs from the RTM we perform full integrations over the atmospheric profiles. Gaussian noise that matches the radiometer use and noise reduction of the resampled TB is added to the computed TB of each channel. This set is then used to train 2-stage regressions. In the 1st stage we regress for a 1st guess of SST and SSWS. In the 2nd stage, we perform separate linear regressions in each (SST, SSWS) bin and linearly interpolate the result to the actual value of the 1st guess parameter. The challenge hereby is to obtain smooth transitions between the different bins.

We train the regressions for a discrete set of EIA using the 37 GHz as reference and computing the EIA angles of the other channel from the WindSat scan geometry when simulating the training TB. For the retrieval, the result is linearly interpolated to the actual 37 GHz EIA.

For retrieving SST, all brightness temperatures are referenced to a common salinity of 35 ppt using the climatology for sea surface salinity and SST from the World Ocean Atlas (WOA98, N.O.D.C, CD-ROM).

The columnar rain rate is computed from the columnar liquid cloud water and SST as in [3].

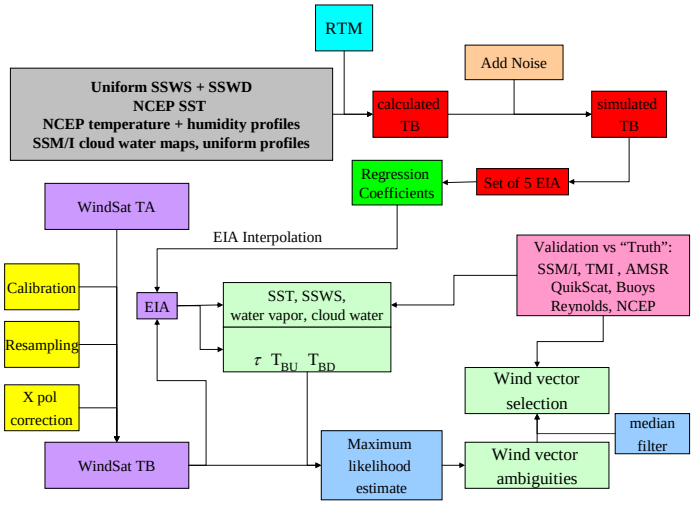

Figure 4. Ocean EDR Algorithm

B. *Maximum Likelihood Estimate (MLE) for Sea Surface Wind Vector*

The retrieval of the sea surface wind vector (SSWS and SSWD) utilizes a MLE of the sum of squares (SOS) between measured and model brightness temperatures:

$$\chi^2 = \sum_{f,i} \frac{\left(T_B^{Measured} - T_B^{Model}\right)_{f,i}}{Var\left[\left(T_B^{Measured} - T_B^{Model}\right)_{f,i}\right]} \qquad (4).$$

The sum runs over all frequencies f with the exception of 6.8 GHz and the following channel combinations i:

- v + h at 10.7, 18.7, 23.8 and 37.0 GHz.

- v – h/2 at 10.7, 18.7, 23.8 and 37.0 GHz.
- 3rd Stokes at 10.7, 18.7 and 37.0 GHz.
- 4th Stokes at 10.7 and 18.7 GHz.

The reason for using the combination v – 0.5h rather than the 2nd Stokes parameter v – h is, that in v – 0.5 h the atmospheric contributions and any associated errors cancel out [6]. The model TB is computed from SST, the atmospheric transmittance and the up and downwelling atmospheric brightness temperatures. Values for those auxiliary parameters are obtained from linear regressions together with SST from section III.A. As the 6.8 GHz is used for retrieving SST, we require all WindSat channels with the exception of 37 L/R to be present for the wind vector retrieval.

The SOS in (4) is divided by the expected variance between measured and model TB. We pre compute this expected variance from the collocated TB – EDR set (section II.A) using our refined RTM (sections II.B, II.C and II.D). TABLE I. shows the result for a global sample of wind speeds. It can be further refined by computing them as function of wind speeds. In the retrieval the expected variance is then linearly interpolated to the wind speed that was obtained from the regression (section III.A). TABLE I. shows clearly that the uncertainties in the combination v-h/2 as well as the 3rd and 4th Stokes are significantly smaller than for v and h itself and therefore they are getting weighted stronger in the MLE.

TABLE I. SQARE ROOT OF EXPECTED VARIANCES [KELVIN].

10 (V+H)/2	0.77
10 V-H/2	0.36
10 3rd Stokes	0.21
10 4th Stokes	0.10
18 (V+H)/2	1.36
18 V-H/2	0.42
18 3rd Stokes	0.32
18 4th Stokes	0.15
23 (V+H)/2	1.81
23 V-H/2	0.47
37 (V+H)/2	2.12
37 V-H/2	0.40
37 3rd Stokes	0.20

C. Ambiguity Selection

The MLE results in a set of 1 – 4 solutions (ambiguities). The average number of ambiguities is 2.7. For selecting an ambiguity we pass the ambiguity array for each orbit through a circular vector median filter (MF), similar to the technique used in scatterometry [9]. This is done separately for forward and aft look.

The median filter cost function has the form:

$$E_{ij}^{k} = \sum_{\substack{m=i-h \\ m\neq i}}^{m=i+h} \sum_{\substack{n=j-h \\ n\neq j}}^{n=j+h} \sqrt{\left(\vec{A}_{ij}^{k} - \vec{U}_{mn}\right)^2} \qquad (5).$$

The window indices *(m, n)* do not include the window centers *(i, j)*. We are using a window size of $h = 7$. Cells that are flagged for rain (columnar liquid cloud water > 0.18 mm) are not included in the MF. The index *k* runs over all ambiguities from 1 up to the total number of ambiguities. $\vec{A}_{ij}^{k}$ is the field, which is currently passed through the filter. The field $\vec{U}_{mn}$ denotes the currently selected ambiguity, which serves as the filter. During each pass the ambiguity $\vec{A}^{k}$ that minimizes the cost function E^{k}, is the newly selected ambiguity. The updating of the selected ambiguity is only done after all cells have been filtered. The median filter is terminated when the relative difference in the cost function of the selected field summed up over all cells, between two consecutive passes is smaller than 10^{-3}.

In a MF without nudging, the filter is initialized with the first ranked ambiguity from the MLE. In a MF with partial nudging, the filter is initialized with the ambiguity that is closest to the space-time interpolated wind vector from NCEP GDAS (or another numerical weather prediction model). In a MF with full nudging, the MF is initialized with the space-time interpolated wind vector from NCEP GDAS (or another numerical weather prediction model).

The wind vector after MF also provides a refined estimate for the scalar SSWS compared with the value that was obtained by regression (section III.A).

IV. VALIDATION OF OCEAN RETRIEVALS

The retrieved ocean EDRs are validated versus the following data sets:

- The WindSat SST are compared with the optimum interpolated Reynolds SST, AMSR-E SST and radiometer measurements from ship cruises.
- The WindSat wind speed, columnar water vapor and columnar liquid cloud water are compared with the observation from satellite microwave imager (SSM/I, TMI, AMSR-E) that is closest in time to the WindSat observation within a 30-minute time window.
- The WindSat wind speed and direction are compared with the observation from QuikScat within a 30 min time window, NCEP GDAS field and buoy observations.

For the validation we apply a rain filter discarding cells for which the columnar liquid cloud water is larger than 0.18 mm. We also filter for sun glitter and RFI.

The results for bias and standard deviations between various data sets are listed in TABLE II. , TABLE III. and TABLE IV.

The comparison of wind directions from WindSat with those from QuikScat and buoys gives values that are very similar than with those from NCEP GDAS in TABLE III.

TABLE II. BIAS AND STANDARD DEVIATION OF SEA SURFACE WIND SPEED (SSWS), WATER VAPOR AND LIQUID CLOUD WATER BETWEEN WINDSAT AND THE COSET IMAGER (SSM/I, TMI, AMSR-E) WITHIN A 30 MINUTE WINDOW.

	SSWS	***Water Vapor***	***Cloud Water***
BIAS	-0.03 m/s	-0.37 mm	-0.008 mm
SDEV	0.77 m/s	0.71 mm	0.018 mm

TABLE III. STANDARD DEVIATION OF SEA SURFACE WIND DIRECTION (SSWD) BETWEEN THE SELECTED AMBIGUITY OF THE WINDSAT FORWARD LOOK AND THE NCEP GDAS FIELD USING A MF WITHOUT NUDGING AND A MF WITH PARTIAL NUDGING.

SSWS bin [m/s]	***SSWD SDEV [deg]***	
	Partial nudge	***No nudge***
0 – 2	72	93
2 - 4	51	80
4 - 6	37	64
6 - 8	22	36
8 - 10	15	20
10 - 12	13	16
12 - 14	11	13
14 - 16	10	12
16 - 18	9	12
> 18	8	10

TABLE IV. BIAS AND STANDARD DEVIATIONS [IN M/S] OF SEA SURFACE WIND SPEED FROM WINDSAT VERSUS CLOSEST IMAGER, QUIKSCAT, BUOYS AND GDAS

	Imager	***QuikScat***	***Buoys***	***GDAS***
BIAS	-0.03	+0.21	+0.17	+0.32
SDEV	0.77	0.66	1.12	1.10

Figure 5. shows a comparison between WindSat SST and those from AMSR-E and OI Reynolds. We have also compared the WindSat SST with data from the MAERI ship cruise, which uses a radiometer to measure the sea surface skin temperature. Other than buoys, which measure the bulk SST between 1 m and 2 m below the sea surface, and which differs from the skin temperature that is measured by the radiometer, the MAERI data can be directly compared with the WindSat measurements as both measure skin SST. The MAERI measurements were taken in warm water (between 24°C and 30°C). A 6 hour time window between MAERI and WindSat measurement was applied and very low winds (below 2 m/s) were discarded to avoid diurnal warming of the sea surface. The bias between WindSat and MAERI SST is -0.30 K, the standard deviation +0.42 K. When compared to Reynolds, AMSR-E and MAERI in warm water, WindSat SSTs show consistently a small cold bias of about 0.3 K, which points to a small residual error in the RTM, that will need to be corrected in the future.

ACKNOWLEDGMENT

We would like to thank Peter Gaiser (NRL, Washington D.C.) for providing us with the WindSat TDRs and antenna pattern correction coefficients. The MAERI SST measurements were provided by Peter Minnett (University of Miami).

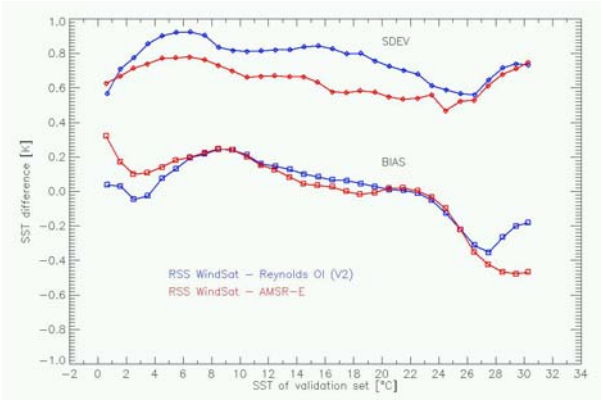

Figure 5. Bias (lower curve) standard deviation (upper curve) between WindSat and AMSR-E (red) and Reynolds (blue) SST.

REFERENCES

[1] F. Wentz and T. Meissner, "AMSR Ocean Algorithm," Algorithm Theoretical Basis Documnt (ATBD), Version 2, RSS Technical Proposal 121599A, Remote Sensing Systems (http://www.remss.com), Santa Rosa, California, December 15, 1999.

[2] R. Reynolds and T. Smith, "Improved global sea surface temperature analyis suing optimum interpolation," Journal of Climate, vol. 7, 1994, pp. 929 – 948.

[3] T. Meissner and F. Wentz, "Polarization rotation and the 3rd Stokes parameter: The effects of spacecraft attitude and Faraday Rotation," IEEE TGARS special WindSat issue, in press.

[4] W. Purdy, P. Gaiser, G. Poe, E. Uliana, T. Meissner and F. Wentz, "Geolocation and pointing accuracy analysis for the WindSat sensor," IEEE TGARS special WindSat issue, in press.

[5] T. Meissner and F. Wentz, "The dielectric constant of pure and sea water from microwave satellite observations," IEEE Trans. Geosci. Remote Sensing, vol. 42(9), 2004, pp. 1836 – 1849.

[6] T. Meissner and F. Wentz, "An updated analysis of the wind direction signal in passive microwave brightness temperatures," IEEE Trans. Geosci. Remote Sensing, vol. 40(6), 2002, pp. 1230 – 1240.

[7] S. Yueh, W. Wilson, S. Dinardo and F. Li, "Polarimetric microwave brightness signatures of ocean wind directions", IEEE Trans. Geosci. Remote Sensing, vol. 37(2), 1999, pp. 949 – 959.

[8] S. Yueh, "Modeling of wind direction signals in polarimetric sea surface brightness temperatures," , IEEE Trans. Geosci. Remote Sensing, vol. 35(6), 1997, pp. 1400 – 1418.

[9] S. Shaffer, S. Dunbar, V. Hsiao and D. Long, "A Median-Filter based ambiguity removal algorithm for NSCAT," IEEE Trans. Geosci. Remote Sensing, vol. 29(1), 1991, pp. 167 – 174.

[10] J. D. Jackson, "Classical Electrodynamics", John Wiley & Sons, New York, 1975.